Research Square

Preprints are preliminary reports that have not undergone peer review.
They should not be considered conclusive, used to inform clinical practice,
or referenced by the media as validated information.

Single-cell transcriptomics reveals anatomical-site-associated immune-stromal remodeling in abdominopelvic NF2-related schwannomatosis

Qiyang Shen
Children's Hospital of Nanjing Medical University
Xiaoci Fan
Nanjing University of Chinese Medicine
Chunlei Zhou
Children's Hospital of Nanjing Medical University
Xinge Li
Nanjing University of Chinese Medicine
Sirui Pan
Children's Hospital of Nanjing Medical University
Nan Xie
Children's Hospital of Nanjing Medical University
Jianfeng Zhou
doctorzhoujianfeng@163.com

Children's Hospital of Nanjing Medical University
Lifeng Zhu
Nanjing University of Chinese Medicine
Tao Li
Children's Hospital of Nanjing Medical University

Article

Keywords: NF2-related schwannomatosis, abdominopelvic schwannoma, single-cell RNA sequencing, fibroblast, macrophage, tumor microenvironment

Posted Date: October 18th, 2026

DOI: https://doi.org/10.21203/rs.3.rs-11138291/v1

License: This work is licensed under a Creative Commons Attribution 4.0 International License.
Read Full License

Additional Declarations: No competing interests reported.

Abstract

NF2-related schwannomatosis (NF2-SWN) is a hereditary tumor-predisposition syndrome caused by pathogenic variants in NF2. Although tumors arising at different anatomical sites share NF2 abnormalities, their biological characteristics may differ. The microenvironment of NF2-SWN-associated abdominopelvic schwannomas remains poorly characterized. We performed single-cell RNA sequencing of abdominopelvic schwannomas from two pediatric patients with NF2-SWN and integrated publicly available datasets of NF2-associated bilateral vestibular schwannomas and normal greater auricular nerves. We identified distinct cellular and transcriptional features across anatomical sites. Abdominopelvic tumors showed attenuated myelination-related programs in Schwann cells, enrichment of TENM2-positive fibroblasts with inflammatory and tissue-remodeling features, and accumulation of CCL3L3-positive inflammation-associated macrophages expressing inflammatory mediators. Cell-cell communication analysis further implicated candidate stromal-myeloid signaling pathways, including CXCL12-CXCR4, CCL3/CCL3L3-CCR1, and TNF signaling. These findings suggest that anatomical context may contribute to immune-stromal remodeling in NF2-SWN and highlight TENM2-positive fibroblasts and CCL3L3-positive macrophages as candidate components of an abdominopelvic inflammatory niche. Given the limited biological replication and computationally inferred interactions, these findings are hypothesis-generating and require validation in larger cohorts and functional studies.

Introduction

NF2-related schwannomatosis (NF2-SWN), previously termed neurofibromatosis type 2, is a rare autosomal-dominant tumor-predisposition syndrome caused predominantly by pathogenic germline variants in the tumor-suppressor gene *NF2* at 22q12.2 [1,2]. *NF2* encodes Merlin, the loss of which perturbs signaling networks including Hippo and mTOR and promotes tumors of the central and peripheral nervous systems [3,4]. NF2-SWN has an estimated prevalence of approximately 1 in 25,000, shows high penetrance, and commonly manifests during adolescence or early adulthood [5]. Bilateral VS is its hallmark and may cause progressive hearing loss, tinnitus, and balance impairment [6,7]. Affected individuals may also develop meningiomas, ependymomas, and ocular abnormalities [8–10]. Current management relies primarily on surveillance, surgery, and radiotherapy. Bevacizumab can achieve tumor control or hearing improvement in a subset of patients with progressive VS, but responses are variable [11–14]. Defining the tissue ecosystems of NF2-associated tumors and identifying potentially actionable mechanisms therefore remain clinically important.

Most NF2-SWN research has focused on VS. NF2-associated schwannomas arising in the retroperitoneum or pelvis are uncommon, and available evidence is largely confined to case reports and small series [15,16]. The relatively compliant abdominopelvic space may permit slow tumor enlargement before symptoms emerge. Patients may present with nonspecific abdominal discomfort or radicular pain, and imaging may demonstrate cystic degeneration, hemorrhage, or calcification [17,18]. Proximity to major vessels and pelvic nerve plexuses can also complicate complete resection [19]. These clinical

differences suggest that, beyond the shared *NF2* abnormality, local tissue context may shape tumor phenotype.

The tumor microenvironment comprises tumor cells, immune cells, stromal cells, and their communication networks. Comparing NF2-associated tumors with similar driver backgrounds but different anatomical origins may help distinguish shared tumor-intrinsic programs from site-associated microenvironmental features. Existing studies, however, remain dominated by VS [20,21], and the cellular composition, stromal states, and immune interactions of abdominopelvic NF2-associated schwannomas have not been systematically defined.

Single-cell RNA sequencing (scRNA-seq) enables tumor heterogeneity to be resolved at cellular resolution. Previous studies have implicated tumor-associated Schwann cells, myeloid cells, and stromal cells in NF2-associated tumor biology [21–24]. Whether distinct anatomical niches reproducibly generate different cell states and communication patterns, particularly in abdominopelvic lesions, remains unknown.

We therefore performed scRNA-seq on abdominopelvic schwannomas from two children with NF2-SWN and integrated these data with public datasets from NF2-associated bilateral VSs and normal greater auricular nerves. We compared major cell populations, Schwann-cell states, fibroblast and myeloid subpopulations, transcriptional regulatory networks, and cell-cell communication. Selected inflammation-related markers were further examined by immunohistochemistry. Our objective was to establish an exploratory single-cell atlas of NF2-associated abdominopelvic schwannomas and generate testable hypotheses regarding their microenvironment.

Results

Clinical cohort and single-cell atlas of NF2-associated abdominopelvic schwannomas

Two boys with NF2-SWN (P1 and P2) were included. P1 was 12 years and 9 months old at presentation. A painless periumbilical mass had been detected 5 years earlier and gradually enlarged, followed by a new subcutaneous scalp mass. Histopathology and immunohistochemistry of a locally excised lesion supported plexiform schwannoma. Subsequent imaging demonstrated a retroperitoneal mass, bilateral vestibular-nerve lesions, and multiple subcutaneous nodules. The resected retroperitoneal lesion was also diagnosed as plexiform schwannoma.

P2 was 9 years and 11 months old and presented with multiple subcutaneous masses. Previously resected lesions from the left shoulder and ankle had been diagnosed as multiple schwannomas. Investigation of gait instability revealed multiple intraspinal masses; a resected lesion was diagnosed as psammomatous meningioma (WHO grade 1). During follow-up, a large pelvic mass was detected and

diagnosed as a cellular schwannoma after resection. Representative imaging demonstrated the abdominopelvic masses and bilateral vestibular-nerve lesions in the two patients (Fig. 1A).

Clinical, radiological, pathological, and molecular findings supported NF2-SWN in both patients. P1 carried a heterozygous *NF2* c.774delG/p.W258X variant, whereas both parents were wild type by Sanger sequencing. P2 carried a heterozygous *NF2* c.1392del/p.E465fs*20 variant that was confirmed as de novo. Both variants were located in the coding region of the principal transcript NM_000268 (Supplementary Fig. S1). Because the protein-level nomenclature in the source diagnostic reports was not standardized according to current HGVS recommendations, the variant descriptions should be rechecked against the original chromatograms and clinical genetics reports before submission.

We performed scRNA-seq on the abdominopelvic tumors and integrated the results with public data from normal greater auricular nerves and NF2-associated bilateral VSs (GSE230375, GSM7809247-GSM7809250). After quality control, 61,480 cells were retained and assigned to 35 clusters. Based on canonical markers, 11 major cell classes were annotated, including T/NK cells (*CD3D*, *CD2*, *GZMA*, and *TRBC2*), myeloid cells (*LYZ* and *C1QC*), fibroblasts (*DCN*, *LUM*, and *COL1A1*), mural cells (*ACTA2*, *TAGLN*, and *MYH11*), endothelial cells (*VWF*, *PECAM1*, *AQP1*, and *CLDN5*), Schwann cells (*NRXN1*, *S100B*, and *CRYAB*), B cells (*MS4A1* and *CD79A*), mast cells, neutrophils, perineurial cells, and proliferating cells (Fig. 1B-D). Descriptively, normal nerves contained large fibroblast, endothelial, and mural-cell compartments; abdominopelvic tumors contained relatively high proportions of myeloid and T/NK cells; and VSs contained the highest proportion of Schwann cells together with a substantial myeloid compartment (Fig. 1E). Because each group comprised only two biological samples and originated from different datasets, these compositional differences were treated as exploratory and were not subjected to cell-level pseudoreplicated inference.

Tumor-associated Schwann cells from abdominopelvic tumors display a low-myelin transcriptional state

Six Schwann-cell subpopulations were identified (Fig. 2A). nmSC_SCN7A was the predominant state across all three groups and was particularly abundant in VS. Myelination-related mSC_MOG and mSC_PRX states were scarce in abdominopelvic tumors (Fig. 2C), suggesting a comparatively low-myelin transcriptional state. Because the normal and tumor samples were obtained from different anatomical locations, this observation alone does not establish active demyelination.

Using T/NK cells as the reference, transcriptome-based CNV inference revealed a chromosome 22 loss-like signal in Schwann cells from both abdominopelvic tumors and VSs. The signal appeared stronger in abdominopelvic tumors, whereas VSs additionally showed a relatively prominent chromosome 12 loss-like signal (Fig. 2B). These findings suggest potential genomic heterogeneity across sites but require DNA-based validation.

Differential-expression and Gene Ontology (GO) analyses of the major nmSC_SCN7A population implicated axonogenesis, gliogenesis, response to transforming growth factor beta, canonical NF-kappaB signaling, extracellular-matrix organization, lymphocyte activation, and chemotaxis in NF2-associated tumor Schwann cells (Fig. 2D). Direct comparison showed that abdominopelvic cells were relatively enriched for chemotaxis, response to fibroblast growth factor, positive regulation of epithelial-cell proliferation and angiogenesis, and response to interleukin-1. VS cells were relatively enriched for myelination, Schwann-cell differentiation, axonogenesis, Wnt signaling, extracellular-matrix organization, and mesenchymal differentiation (Fig. 2E). These enrichment results represent transcriptional associations and do not establish pathway activity or causality.

Candidate genes from the nmSC_SCN7A analysis were evaluated in an external nerve-sheath tumor cohort. High *NCAM1* expression was associated with shorter overall survival, whereas high *ITGB4* expression was associated with longer overall survival (Fig. 2F). Because the external cohort did not fully match the present cohort in histological composition, disease stage, or *NF2* status, this analysis was used only for candidate prioritization and should not be interpreted as NF2-SWN-specific or independent prognostic evidence.

TENM2-positive inflammation-associated fibroblasts are enriched in abdominopelvic tumors

Six fibroblast subpopulations were identified, with distinct compositional patterns across groups (Fig. 3A). Normal nerves predominantly contained SFRP2-positive, MYOC-positive, PCOLCE2-positive, and MYH11-positive fibroblasts. TENM2-positive fibroblasts were derived almost exclusively from abdominopelvic samples, whereas CLDN11-positive fibroblasts were largely restricted to VSs (Fig. 3B). Because subpopulation identity strongly overlapped with data source, anatomical-site effects could not be fully separated from cohort, batch, and patient effects.

UCell scoring indicated that fibroblasts from abdominopelvic tumors had relatively high inflammatory, myofibroblast-like, and pro-epidermal-growth scores, whereas VS-derived fibroblasts showed a higher extracellular-matrix-remodeling score (Fig. 3C). At the subpopulation level, TENM2-positive fibroblasts showed concurrent enrichment of inflammatory and pro-epidermal-growth signatures (Fig. 3D,E), consistent with an inflammation-associated stromal state.

Intersecting epidermal-growth-related genes, inflammation-related genes, and genes differentially expressed in TENM2-positive fibroblasts yielded eight candidates (Fig. 3F). Among them, *CLDN1*, *NRP2*, and *TENM2* showed relatively clear overexpression in abdominopelvic samples. *H3-3A*, *H3-3B*, and *RPS4Y1* also differed among groups, whereas *ECRG4* and *PHLDA1* showed more complex patterns (Fig. 3G). This procedure prioritizes candidate markers but does not demonstrate a functional driver role.

Pseudotime analysis placed most normal-nerve fibroblasts toward one end of the trajectory, whereas abdominopelvic- and VS-derived fibroblasts occupied distinct terminal branches. *TENM2* and *NRP2*

increased along the abdominopelvic-associated branch (Fig. 4A,B). This inferred trajectory suggests state continuity but should not be interpreted as an experimentally validated lineage relationship.

pySCENIC identified EGR3, SRF, BHLHE41, KLF10, and FOXP2 regulons as relatively active in abdominopelvic fibroblasts (Fig. 4C). Their predicted targets were enriched in Wnt signaling, axonogenesis, chemotaxis, neurogenesis, response to transforming growth factor beta, canonical NF-kappaB signaling, mesenchymal differentiation, response to tumor necrosis factor, epithelial-cell proliferation, epithelial-mesenchymal transition, PI3K-AKT signaling, fibroblast proliferation, and angiogenesis (Fig. 4D). Immunohistochemical analysis revealed that TENM2 and NRP2 were expressed to varying degrees in NF2-associated tumours of the abdominal and pelvic regions, the shoulder and the cranium; TENM2 was expressed more strongly in samples from two paediatric patients with abdominal and pelvic tumours (Fig. S1). These regulons may contribute to the inflammatory and tissue-remodeling state of TENM2-positive fibroblasts, but direct regulatory relationships require chromatin and perturbation experiments.

CCL3L3-positive inflammation-associated macrophages are enriched in abdominopelvic tumors

Among myeloid cells, 19,930 macrophages were identified and subdivided into nine populations (Fig. 5A). RNASE1-positive macrophages predominated in normal nerves, CCL3L3-positive macrophages predominated in abdominopelvic tumors, and PLCG2-positive and CCL3L1-positive macrophages were abundant in VSs, which also contained increased HSPA1A-positive, FCGBP-positive, and VEGFA-positive populations (Fig. 5B).

UCell scores showed variable inflammatory, lipid-metabolic, tissue-resident-like, proangiogenic, proliferative, interferon-response, immunoregulatory, and extracellular-matrix-remodeling programs across macrophage states (Fig. 5C). At the group level, macrophages from abdominopelvic tumors had relatively high proinflammatory, proliferative, and proangiogenic scores, whereas VS-derived macrophages had a higher interferon-response score. Macrophages from both tumor types showed enhanced lipid-metabolic, matrix-remodeling, and immune-response programs, whereas normal-nerve macrophages were more tissue-resident-like (Fig. 5D).

CCL3L1-positive, CCL3L3-positive, and VEGFA-positive populations had high proinflammatory scores (Fig. 5E,F) and were operationally combined as inflammation-associated macrophages; all remaining populations were classified as other macrophages (Fig. 5G). Relative to other macrophages, inflammation-associated macrophages upregulated inflammatory or chemotactic mediators including *IL1B*, *IL1A*, *CCL3L3*, *TNF*, and *CXCL8*, together with stress-feedback or survival-associated genes including *DUSP2*, *TNFAIP3*, and *BCL2A1* (Fig. 5H and Fig. 6A). This transcriptional combination supports sustained inflammatory stress but is insufficient to define a stable M1 phenotype.

Immunohistochemistry demonstrated variable expression of IL1B, CCL3L3, CXCL8, and TNFAIP3 in abdominopelvic, shoulder, and intracranial NF2-associated tumors (Fig. 6B). Because the figures did not provide standardized quantitative scores and the staining patterns were not uniform across markers and sites, these data confirm tissue expression and intersite heterogeneity but do not establish consistent upregulation in abdominopelvic tumors.

Compared with VS-derived macrophages, genes upregulated in abdominopelvic macrophages were enriched in positive regulation of cell activation, regulation of inflammatory responses, canonical NF-kappaB signaling, response to tumor necrosis factor, regulation of chemotaxis, macrophage activation, and cytokine production (Fig. 6C). In addition, monocytes from abdominopelvic tumors showed a higher NF-kappaB-related inflammatory-response score than those from VSs (Fig. 6D). Together, these findings indicate a comparatively strong inflammation-associated myeloid program in abdominopelvic samples that may contribute to local immune recruitment and microenvironmental remodeling.

Cell-cell communication inference identifies candidate stromal-myeloid interaction networks

CellChat was used to compare potential communication among tissue sources, including both secreted and contact-dependent signals. Ligand-receptor analysis estimates communication probabilities from expression data and does not provide direct evidence of molecular interaction.

Relative and absolute information-flow analyses showed prominent IL1, BTLA, CTSG, and IGF signaling in normal nerves; TNF, IL16, ANGPT, and CCL signaling in abdominopelvic tumors; and COMPLEMENT, SPP1, PERIOSTIN, and NRG signaling in VSs. MIF, GALECTIN, CXCL, and CypA signaling remained prominent across all groups (Fig. 7A). Network visualization further suggested broad involvement of fibroblasts, inflammation-associated macrophages, monocytes, and other populations in MIF, CCL, CXCL, and TNF signaling (Fig. 7B).

Among fibroblast-associated ligand-receptor pairs, both NF2-associated tumor types showed MIF-receptor-complex and CCL3-CCR1 communication. Abdominopelvic tumors additionally showed strong CXCL12-CXCR4 and myeloid-directed CCL3L3-CCR1 communication (Fig. 7C). Group-level expression was broadly consistent with these predictions: *CCL3L3* was almost selectively elevated in abdominopelvic samples, *CXCL12* was higher in abdominopelvic tumors than in VSs, and *MIF* was elevated in both tumor groups (Fig. 7D).

Analysis centered on inflammation-associated macrophages identified increased communication probabilities for MIF-CD74/CD44, MIF-CD74/CXCR4, TNF-TNFRSF1B, and CCL3/CCL3L3-CCR1 in abdominopelvic samples (Fig. 7E,F). Together with *TNF* and *CCL3L3* expression in this population, these signals may contribute to myeloid recruitment and maintenance of inflammatory states, but spatial colocalization and functional blockade experiments are required.

Among contact-dependent signals, MPZ- and NRXN-related communication predominantly involved Schwann and perineurial cells. NRXN signaling was retained in both tumor groups, whereas MPZ-related communication and *MPZ* expression were weaker in abdominopelvic samples, consistent with their low-myelin transcriptional state (Fig. 7G,H). CLDN signaling further suggested site-dependent patterns of fibroblast interactions with immune or perineurial cells (Fig. 7G). These data raise the possibility of anatomical-site-associated remodeling of cell-junction and local barrier programs.

Discussion

We generated an exploratory single-cell atlas of NF2-SWN-associated abdominopelvic schwannomas and compared it with public data from NF2-associated VSs and normal nerves. Abdominopelvic tumor-associated Schwann cells displayed a low-myelin transcriptional state; TENM2-positive fibroblasts and CCL3L3-positive inflammation-associated macrophages were enriched in abdominopelvic samples; and expression-based communication analyses implicated CXCL12-CXCR4, MIF receptor complexes, CCL3/CCL3L3-CCR1, and TNF-receptor networks as candidate links between stromal and myeloid compartments. These findings support a working model in which a shared *NF2* abnormality and local tissue context jointly shape the tumor microenvironment, while highlighting the confounding inherent in comparisons across anatomical sites and independent cohorts.

Schwann cells are the principal neoplastic population in NF2-associated schwannomas, and loss of Merlin can induce broad signaling and cell-state changes. *NF2* inactivation has been linked to dysregulated Hippo, PI3K-AKT, MAPK, and NF-kappaB networks[12]. In our data, the major nmSC_SCN7A population from both abdominopelvic tumors and VSs exhibited neural-remodeling, inflammatory, and extracellular-matrix-associated programs, indicating a shared core transcriptional alteration.

Abdominopelvic samples also showed lower *MPZ* expression, weaker MPZ-related communication, and fewer myelination-related Schwann-cell populations. MPZ is a major structural protein of mature myelinating Schwann cells, and reduced expression can reflect attenuation of differentiation or nerve-support programs [25,26]. Cross-sectional scRNA-seq, however, cannot distinguish pre-existing anatomical differences from tumor-associated dedifferentiation or active demyelination. We therefore interpret the finding conservatively as a low-myelin transcriptional state. Its association with inflammatory, chemotactic, and angiogenic programs raises the possibility that Schwann cells participate in microenvironmental remodeling [27–31], although temporal or intervention studies are required to determine whether they act upstream of stromal and immune changes.

The most prominent stromal feature of abdominopelvic samples was enrichment of TENM2-positive fibroblasts. Tumor-associated fibroblasts not only produce extracellular matrix but also regulate immune-cell recruitment and tissue remodeling through cytokines, chemokines, and growth factors [32–37]. The TENM2-positive population displayed inflammatory, pro-epidermal-growth, and chemotactic programs, suggesting an inflammation-associated stromal state in NF2 abdominopelvic tumors.

TENM2 encodes a teneurin-family transmembrane protein involved in cell adhesion, neural development, and intercellular communication [38,39], and aberrant expression has been described in several cancers [40,41]. The present data are insufficient to define TENM2 as a functional driver. A more defensible interpretation is that TENM2 marks this fibroblast state, while *CLDN1*, *NRP2*, and other coexpressed genes may reflect its localization and communication properties. Importantly, the supplied result figures did not include tissue-level validation of TENM2 or NRP2; conclusions regarding these markers should therefore remain confined to the single-cell transcriptomic level.

pySCENIC suggested enhanced EGR3, SRF, BHLHE41, KLF10, and FOXP2 programs in abdominopelvic fibroblasts. EGR3 can respond to inflammatory stimuli and regulate genes such as *IL6* and *IL8* [42,43], and it participates in immune and tissue-stress responses [44,45]. EGR3 may therefore link local stress to the observed inflammation-associated stromal state. Because SCENIC infers regulatory relationships from coexpression and motif information, validation by chromatin-accessibility, transcription-factor binding, or genetic perturbation experiments is needed.

Abdominopelvic samples were also enriched in CCL3L3-positive inflammation-associated macrophages expressing *IL1B*, *CXCL8*, and *TNF*, together with feedback or survival genes including *TNFAIP3*, *DUSP2*, and *BCL2A1*. This profile is consistent with sustained inflammatory stress but should not be equated with a fixed M1 phenotype. Inflammation-associated macrophages can influence immune recruitment, angiogenesis, and matrix remodeling through cytokines, chemokines, and repair signals [46,47], yet their net effect on NF2-associated tumor growth remains unresolved. Immunohistochemistry confirmed tissue expression of candidate inflammatory molecules but also revealed substantial intersite heterogeneity. Without blinded quantification and validation in a larger cohort, these images should not be interpreted as evidence of abdominopelvic-specific upregulation.

Cell-cell communication analysis provided further clues to stromal-myeloid crosstalk. Abdominopelvic samples showed increased probabilities for MIF receptor complexes, CXCL12-CXCR4, and CCL3L3-CCR1 between fibroblasts and myeloid cells. MIF and CXCL12-CXCR4 can regulate myeloid-cell migration, retention, and functional states [46,48–53]. Predicted TNF-TNFRSF1A/TNFRSF1B, MIF-CD74/CD44 or MIF-CD74/CXCR4, and CCL3/CCL3L3-CCR1 networks further suggest that inflammation-associated macrophages may serve as a signal-maintenance node [54–60]. Ligand and receptor coexpression, however, does not prove signal transmission, and the effects of MIF on myeloid states are context dependent. These pathways should therefore be regarded as candidate communication hubs rather than established unidirectional proinflammatory drivers.

Taken together, our data support a testable model in which *NF2*-associated Schwann-cell alterations and the abdominopelvic tissue context coincide with enrichment of TENM2-positive fibroblasts and CCL3L3-positive inflammation-associated macrophages. CXCL12, MIF, CCL3/CCL3L3, and TNF networks may help sustain stromal-myeloid interactions. This model integrates the transcriptomic and immunohistochemical observations but does not establish temporal order or causality.

From a translational perspective, CXCL12-CXCR4, MIF receptor complexes, and TNF-receptor signaling represent priorities for mechanistic validation [50,61,62]. Before therapeutic implications are considered, their reproducibility should be established in larger NF2-SWN cohorts, and the net effects of pathway blockade on tumor cells, normal peripheral nerves, and immune cells should be assessed.

This study has several limitations. First, the abdominopelvic cohort comprised only two patients, while normal nerves and VSs were obtained from public datasets. Anatomical origin, library preparation, batch, and interpatient differences may therefore be confounded with disease or site effects, and large cell numbers do not substitute for biological replication. Second, the normal greater auricular nerve is not an anatomically matched control for abdominopelvic nerves. Third, CNV, pseudotime, regulon activity, and cell-cell communication were computationally inferred and do not directly establish genomic events, lineage relationships, or signal transmission. Fourth, immunohistochemical validation was limited and lacked uniform quantitative scoring, blinded assessment, and replication in an independent cohort. Fifth, the external survival cohort did not fully match the pathological composition of NF2-SWN, and its provenance must be reported before submission. Future work should include larger multicenter cohorts, patient-level statistical models, spatial profiling, DNA-based validation, and in vitro and in vivo functional experiments.

Materials and methods

Clinical samples and ethical approval

The protocol for research involving human samples was approved by the ethics committee of the Children's Hospital of Nanjing Medical University and conducted in accordance with the Declaration of Helsinki and relevant regulations. Written informed consent was obtained from the legal guardians of both participants. Two pediatric patients with NF2-SWN diagnosed by clinical, radiological, pathological, and molecular criteria were included. Both had bilateral VSs and abdominopelvic schwannomas. Fresh surgically resected abdominopelvic tumor tissue was collected for scRNA-seq, and corresponding formalin-fixed, paraffin-embedded samples were collected for immunohistochemistry. Patient information was deidentified for analysis and reporting.

Tissue dissociation and single-cell suspension preparation

Fresh tissue was placed in ice-cold calcium- and magnesium-free 1× PBS. Gross blood and adipose tissue were removed, and samples were minced into approximately 0.5-mm² fragments. Tissue was digested for 20 min at 37°C with agitation at 100 rpm in a solution containing 0.35% collagenase IV, 2 mg/mL papain, and 120 U/mL DNase I. Digestion was terminated with PBS containing 10% fetal bovine serum, followed by gentle trituration 5–10 times. Cell suspensions were sequentially passed through 70- and 30-μm strainers and centrifuged at 300 × g for 5 min at 4°C. After red-blood-cell lysis, dead cells were removed using the Dead Cell Removal Kit (Miltenyi Biotec, cat. no. 130-090-101). Cells were washed twice and resuspended in PBS containing 0.04% bovine serum albumin. Viability was assessed

by trypan-blue exclusion and was required to exceed 85%. Cells were counted using a Countess II automated cell counter and adjusted to 700-1,200 cells/μL.

10x Genomics library construction and sequencing

Cells were loaded according to the manufacturer's instructions for the 10x Genomics Chromium Single Cell 3' Gene Expression v3 kit, targeting approximately 5,000 captured cells per sample. Following cDNA amplification and library preparation, paired-end 150-bp sequencing was performed on an Illumina NovaSeq 6000 at a depth of at least 20,000 reads per cell.

Single-cell data preprocessing, integration, and annotation

Demultiplexing and FASTQ generation were performed using bcl2fastq v2.20. Cell Ranger v3.1.0 was used for barcode processing, unique molecular identifier counting, and alignment to the human GRCh38 reference genome. Expression matrices were imported into Seurat for quality control and downstream analyses. Genes detected in fewer than three cells were excluded. Cells with > 500 detected genes, > 500 unique molecular identifiers, and < 25% mitochondrial transcripts were retained. After quality control and integration, 61,480 cells were analyzed.

Data were normalized using LogNormalize, highly variable genes were identified, and principal-component analysis was performed. The first 10 principal components were used to construct a shared-nearest-neighbor graph and perform clustering, and uniform manifold approximation and projection was used for visualization. Cluster markers were identified using FindAllMarkers and the Wilcoxon rank-sum test. Candidate markers were required to be expressed in > 10% of cells in the corresponding cluster, have an average log2 fold change > 0.25, and pass multiple-testing correction. Cell types were manually annotated using canonical markers and published literature.

Differential-expression and functional-enrichment analyses

Differential expression was assessed using Seurat FindMarkers and the Wilcoxon rank-sum test. Candidate differentially expressed genes were required to be detected in > 10% of cells in at least one comparison group, have an absolute average log2 fold change > 0.25, and have a Bonferroni-adjusted *P* value < 0.05. Given the limited number of biological samples, cell-level *P* values were used only for feature prioritization and were interpreted together with effect sizes, detection rates, and consistency across patients.

GO and Kyoto Encyclopedia of Genes and Genomes enrichment analyses were conducted using clusterProfiler v4.14.6. *P* values were adjusted by the Benjamini-Hochberg procedure, and adjusted $P < 0.05$ was considered significant. Terms were displayed according to direction of effect, biological relevance, and redundancy reduction.

Subclustering and UCell scoring

Schwann cells, fibroblasts, myeloid cells, and T/NK cells were separately extracted and reprocessed using normalization, dimensionality reduction, and clustering procedures consistent with the global analysis. A clustering resolution of 0.8 was used, and subpopulations were named according to marker expression and functional features. UCell v2.10.1 was used to score predefined gene sets at single-cell resolution. The source and complete membership of all gene sets should be provided in the Supplementary Information.

Pseudotime and transcriptional-regulatory-network analyses

Fibroblast trajectories were reconstructed using Monocle2 v2.34.0. The top 2,000 highly variable genes identified in Seurat were used as ordering genes, DDRTree was used for dimensionality reduction, and plot_cell_trajectory was used to visualize cell states and candidate-gene expression along pseudotime. The trajectory root was assigned according to the distribution of homeostatic fibroblasts from normal nerves. Pseudotime was interpreted as a potential continuum of states rather than direct lineage evidence.

Transcriptional regulatory networks were inferred using pySCENIC v0.12.1. GRNBoost2 was first used to infer regulator-target coexpression networks, followed by cisTarget motif enrichment and removal of indirect targets. Regulon activity in each cell was quantified using AUCell, and the Regulon Specificity Score was used to identify population-specific regulons.

CNV inference from scRNA-seq data

Large-scale CNVs in Schwann cells were inferred using inferCNV, with T/NK cells as the reference. Genes expressed in at least 20 cells were ordered by chromosomal position, and relative expression was smoothed using a 101-gene sliding window. Heatmaps were generated from chromosome-arm or whole-chromosome inference signals. Because schwannomas are generally benign, the target cells are referred to as tumor-associated Schwann cells, and all CNV results are interpreted as transcriptome-based inferences.

Cell-cell communication analysis

Ligand-receptor communication was inferred using CellChat v2.1.2. Separate CellChat objects were constructed for each tissue source, and the human ligand-receptor database was used to estimate communication probabilities and pathway-level information flow. Secreted and contact-dependent signaling were compared. Only cell populations meeting a prespecified minimum cell count were retained, and key ligand-receptor pairs were cross-checked against ligand and receptor expression distributions.

Exploratory survival analysis

RNA-seq expression matrices and clinical follow-up data for a publicly available nerve-sheath tumor cohort were downloaded. Expression and clinical records were merged by unique patient identifier after

duplicate samples, follow-up time, and endpoint definitions had been checked. Patients were divided into high- and low-expression groups at the median expression of each candidate gene. Overall survival was estimated using the Kaplan-Meier method and compared by the log-rank test with the R packages survival and survminer. Because the external cohort may include pathological entities biologically distinct from NF2-SWN, results were considered exploratory and were not extrapolated as disease-specific evidence.

Immunohistochemistry

NF2-SWN-associated tumor tissues from different anatomical sites were fixed in 4% paraformaldehyde, routinely dehydrated, paraffin embedded, and sectioned at 5 μm. Sections were deparaffinized, rehydrated, subjected to antigen retrieval, blocked, and treated to quench endogenous peroxidase activity. Primary antibodies were applied at 1:100 overnight at 4°C. After PBS washing, appropriate secondary antibodies were applied for 1 h at room temperature. Signals were developed using diaminobenzidine, and nuclei were counterstained with hematoxylin. Images were acquired using an Olympus light microscope at 200× and 400× magnification.

Statistical analysis

Unless otherwise specified, single-cell differential expression was assessed using the Wilcoxon rank-sum test with multiple-testing correction, enrichment analyses used Benjamini-Hochberg adjustment, and survival curves were compared using the log-rank test. All tests were two-sided, and adjusted $P < 0.05$ was considered significant. Because biological sample numbers were limited, cell-level analyses were used for description and candidate discovery, and individual cells were not treated as independent biological replicates.

Declarations

Author contributions

Conceptualization, Q.S., X.F., C.Z. and X.L.; methodology, Q.S., X.F. and C.Z.; investigation, Q.S., X.F., C.Z., X.L., S.P. and N.X.; writing-original draft, Q.S., X.F. and C.Z.; writing-review and editing, X.L., S.P., N.X., J.Z., L.Z. and T.L.; funding acquisition, T.L., J.Z. and L.Z.; resources, X.L., J.Z. and L.Z.; supervision, J.Z., L.Z. and T.L.

Data and code availability

The public single-cell dataset reanalyzed in this study is available from the Gene Expression Omnibus under accession GSE230375 (GSM7809247-GSM7809250). The raw data of the sequences have been submitted to BioProject(BioProject - CNCB-NGDC),under accession number PRJCA074602.

Ethics statement

This study was approved by the ethics committee of the Children's Hospital of Nanjing Medical University; the approval number should be added before submission (Approval number: 202505035- 1). Written informed consent was obtained from the legal guardians of both participants.

References

1. International Consensus Group on Neurofibromatosis Diagnostic, C. *et al.* Updated diagnostic criteria and nomenclature for neurofibromatosis type 2 and schwannomatosis: An international consensus recommendation. *Genetics in Medicine* **24**, 1967-1977, doi:10.1016/j.gim.2022.05.007 (2022).
2. Kresak, J. L. & Walsh, M. Neurofibromatosis: A Review of NF1, NF2, and Schwannomatosis. *J Pediatr Genet* **5**, 98-104, doi:10.1055/s-0036-1579766 (2016).
3. Halliday, D., Parry, A. & Evans, D. G. Neurofibromatosis type 2 and related disorders. *Current Opinion in Oncology* **31**, 562-567, doi:10.1097/CCO.0000000000000579 (2019).
4. Ardern-Holmes, S., Fisher, G. & North, K. Neurofibromatosis Type 2: Presentation, Major Complications, and Management, With a Focus on the Pediatric Age Group. *Journal of Child Neurology* **32**, 9-22, doi:10.1177/0883073816666736 (2016).
5. Lee, T. J., Chopra, M., Kim, R. H., Parkin, P. C. & Barnett-Tapia, C. Incidence and prevalence of neurofibromatosis type 1 and 2: a systematic review and meta-analysis. *Orphanet J Rare Dis* **18**, 292, doi:10.1186/s13023-023-02911-2 (2023).
6. Ruggieri, M. *et al.* Childhood neurofibromatosis type 2 (NF2) and related disorders: from bench to bedside and biologically targeted therapies. *Acta Otorhinolaryngol Ital* **36**, 345-367, doi:10.14639/0392-100x-1093 (2016).
7. Wang, M. X. *et al.* Neurofibromatosis from Head to Toe: What the Radiologist Needs to Know. *RadioGraphics* **42**, 1123-1144, doi:10.1148/rg.210235 (2022).
8. Le, C., Thomas, A. & Lui, F. in *StatPearls* (StatPearls Publishing Copyright © 2026, StatPearls Publishing LLC., 2026).
9. Habibi, M. A., Mirjani, M. S., Ahmadvand, M. H., Delbari, P. & Alasti, O. The safety and efficacy of dabrafenib and trametinib in patients with glioma: A systematic review and meta-analysis. *Eur J Clin Pharmacol* **80**, 639-656, doi:10.1007/s00228-024-03635-3 (2024).
10. Rai., -. P. *et al.* Classification of schwannomas and the new naming convention for “neurofibromatosis-2”: Genetic updates and international consensus recommendation. *The Neuroradiology Journal* **38(2025)**, 533-542, doi:doi: 10.1177/19714009251313510 (2025).
11. Cumpston, E. C., Rhodes, S. D. & Yates, C. W. Advances in Targeted Therapy for Neurofibromatosis Type 2 (NF2)-Associated Vestibular Schwannomas. *Curr Oncol Rep* **25**, 531-537, doi:10.1007/s11912-023-01388-3 (2023).

12. Jiramongkolchai, P., Schwartz, M. S. & Friedman, R. A. Management of Neurofibromatosis Type 2-Associated Vestibular Schwannomas. *Otolaryngol Clin North Am* **56**, 533-541, doi:10.1016/j.otc.2023.02.012 (2023).
13. Renzi, S. *et al.* Bevacizumab for NF2-associated vestibular schwannomas of childhood and adolescence. *Pediatr Blood Cancer* **67**, e28228, doi:10.1002/pbc.28228 (2020).
14. Park, S., Woo, T. G., Kang, S. M., Kim, B. H. & Park, B. J. Emerging Molecular Insights and Therapeutic Directions in Neurofibromatosis Type 1 and NF2-Related Schwannomatosis. *Int J Mol Sci* **27**, doi:10.3390/ijms27062867 (2026).
15. Peyre, M. Surgical management of sporadic and schwannomatosis-associated dumbbell cervical schwannomas. *Neurochirurgie* **72**, 101868, doi:https://doi.org/10.1016/j.neuchi.2026.101868 (2026).
16. Kawsar, K. A., Haque, M. R. & Chowdhury, F. H. Abdominal schwannoma in a case of neurofibromatosis type 2: A report of a rare combination. *Asian J Neurosurg* **12**, 89-91, doi:10.4103/1793-5482.145347 (2017).
17. Group, T. A. R. S. W. Intercontinental collaborative experience with abdominal, retroperitoneal and pelvic schwannomas. *BJS (British Journal of Surgery)* **107**, 452-463, doi:https://doi.org/10.1002/bjs.11376 (2020).
18. Hafez, B. *et al.* Neurofibromatosis Type 2 Presenting as Symptomatic Gallbladder Hydrops: A Rare Case Report and Literature Review. *Case Reports in Pediatrics* **2024**, 7680840, doi:https://doi.org/10.1155/crpe/7680840 (2024).
19. Kunugitani, K. *et al.* Malignant perineurioma derived from the retroperitoneum with an aggressive clinical course: a case report. *Surgical Case Reports* **10**, 121, doi:10.1186/s40792-024-01915-9 (2024).
20. Coy, S., Rashid, R., Stemmer-Rachamimov, A. & Santagata, S. An update on the CNS manifestations of neurofibromatosis type 2. *Acta Neuropathol* **139**, 643-665, doi:10.1007/s00401-019-02029-5 (2020).
21. Zhao, F. *et al.* Multiplatform molecular analyses reveal two molecular subgroups of NF2-related schwannomatosis vestibular schwannomas with distinct tumour microenvironment and therapeutic vulnerabilities. *Acta Neuropathologica* **149**, 47, doi:10.1007/s00401-025-02883-6 (2025).
22. Wang, Y. *et al.* Single-cell and spatial transcriptomics analyses reveal tumor microenvironment–driven proliferation of NF2-associated vestibular schwannomas. *Journal of Neuroinflammation* **23**, 165, doi:10.1186/s12974-026-03799-y (2026).
23. Stylianides, C. *et al.* Epigenetic Mechanisms in Neurofibromatosis Types 1 and 2. *Epigenomes* **9** (2025).
24. Wang, X. *et al.* WWC proteins–mediated compensatory mechanism restricts schwannomatosis driven by NF2 loss of function. *Science Advances* **11**, eadp4765, doi:doi:10.1126/sciadv.adp4765 (2025).

25. Salzer, J. L. Schwann cell myelination. *Cold Spring Harb Perspect Biol* **7**, a020529, doi:10.1101/cshperspect.a020529 (2015).
26. Fridman, V. & Saporta, M. A. Mechanisms and Treatments in Demyelinating CMT. *Neurotherapeutics* **18**, 2236-2268, doi:10.1007/s13311-021-01145-z (2021).
27. Liao, C. P. *et al.* Contributions of inflammation and tumor microenvironment to neurofibroma tumorigenesis. *J Clin Invest* **128**, 2848-2861, doi:10.1172/jci99424 (2018).
28. Heredia, J. E. *et al.* Single-Cell Transcriptomic Analysis Links Nonmyelinating Schwann Cells to Proinflammatory Response in the Lung. *The Journal of Immunology* **211**, 844-852, doi:10.4049/jimmunol.2200946 (2023).
29. Hammond, B. P., Panda, S. P., Kaushik, D. K. & Plemel, J. R. in *Microglia: Physiology, Pathophysiology and Therapeutic Potential* (eds Marie-Ève Tremblay & Alexei Verkhratsky) 445-456 (Springer International Publishing, 2024).
30. He, K., Wang, H., Huo, R., Jiang, S.-H. & Xue, J. Schwann cells and enteric glial cells: Emerging stars in colorectal cancer. *Biochimica et Biophysica Acta (BBA) - Reviews on Cancer* **1879**, 189160, doi:https://doi.org/10.1016/j.bbcan.2024.189160 (2024).
31. Trias, E. *et al.* Schwann cells orchestrate peripheral nerve inflammation through the expression of CSF1, IL-34, and SCF in amyotrophic lateral sclerosis. *Glia* **68**, 1165-1181, doi:10.1002/glia.23768 (2020).
32. Xiang, X. *et al.* Cancer-associated fibroblasts: Vital suppressors of the immune response in the tumor microenvironment. *Cytokine & Growth Factor Reviews* **67**, 35-48, doi:https://doi.org/10.1016/j.cytogfr.2022.07.006 (2022).
33. Ganguly, D. *et al.* Cancer-Associated Fibroblasts: Versatile Players in the Tumor Microenvironment. *Cancers (Basel)* **12**, doi:10.3390/cancers12092652 (2020).
34. Kalluri, R. The biology and function of fibroblasts in cancer. *Nat Rev Cancer* **16**, 582-598, doi:10.1038/nrc.2016.73 (2016).
35. Ershaid, N. *et al.* NLRP3 inflammasome in fibroblasts links tissue damage with inflammation in breast cancer progression and metastasis. *Nat Commun* **10**, 4375, doi:10.1038/s41467-019-12370-8 (2019).
36. Mao, X. *et al.* Crosstalk between cancer-associated fibroblasts and immune cells in the tumor microenvironment: new findings and future perspectives. *Mol Cancer* **20**, 131, doi:10.1186/s12943-021-01428-1 (2021).
37. Takahashi, H. *et al.* Cancer-associated fibroblasts promote an immunosuppressive microenvironment through the induction and accumulation of protumoral macrophages. *Oncotarget* **8**, 8633-8647, doi:10.18632/oncotarget.14374 (2017).
38. Wides, R. The Natural History of Teneurins: A Billion Years of Evolution in Three Key Steps. *Frontiers in Neuroscience* **13**, 109, doi:10.3389/fnins.2019.00109 (2019).
39. Rebolledo-Jaramillo, B. & Ziegler, A. Teneurins: An Integrative Molecular, Functional, and Biomedical Overview of Their Role in Cancer. *Frontiers in Neuroscience* **Volume 12 - 2018**,

doi:10.3389/fnins.2018.00937 (2018).

40. Suzuki, H. *et al.* DNA Methylation in Noncancerous Liver Tissues as Biomarker for Multicentric Occurrence of Hepatitis C Virus-Related Hepatocellular Carcinoma. *Gastro Hep Adv* **1**, 555-562, doi:10.1016/j.gastha.2022.02.016 (2022).
41. Min, Y. *et al.* Single extracellular vesicle surface protein-based blood assay identifies potential biomarkers for detection and screening of five cancers. *Molecular Oncology* **18**, doi:10.1002/1878-0261.13586 (2024).
42. Külp, M. *et al.* The EGR3 regulome of infant KMT2A-r acute lymphoblastic leukemia identifies differential expression of B-lineage genes predictive for outcome. *Leukemia* **37**, 1216-1233, doi:10.1038/s41375-023-01895-z (2023).
43. Baron, V. T., Pio, R., Jia, Z. & Mercola, D. Early Growth Response 3 regulates genes of inflammation and directly activates IL6 and IL8 expression in prostate cancer. *Br J Cancer* **112**, 755-764, doi:10.1038/bjc.2014.622 (2015).
44. Knudsen, A. M. *et al.* Expression and prognostic value of the transcription factors EGR1 and EGR3 in gliomas. *Scientific Reports* **10**, 9285, doi:10.1038/s41598-020-66236-x (2020).
45. Shin, S. H., Kim, I., Lee, J. E., Lee, M. & Park, J. W. Loss of EGR3 is an independent risk factor for metastatic progression in prostate cancer. *Oncogene* **39**, 5839-5854, doi:10.1038/s41388-020-01418-5 (2020).
46. Qin, R. *et al.* Role of chemokines in the crosstalk between tumor and tumor-associated macrophages. *Clinical and Experimental Medicine* **23**, 1359-1373, doi:10.1007/s10238-022-00888-z (2023).
47. Figueiredo, C. R. *et al.* Blockade of MIF-CD74 Signalling on Macrophages and Dendritic Cells Restores the Antitumour Immune Response Against Metastatic Melanoma. *Front Immunol* **9**, 1132, doi:10.3389/fimmu.2018.01132 (2018).
48. Xie, J. *et al.* Single-cell histone chaperones patterns guide intercellular communication of tumor microenvironment that contribute to breast cancer metastases. *Cancer Cell International* **23**, 311, doi:10.1186/s12935-023-03166-4 (2023).
49. Peng, Z. *et al.* Interactions between MFAP5 + fibroblasts and tumor-infiltrating myeloid cells shape the malignant microenvironment of colorectal cancer. *J Transl Med* **21**, 405, doi:10.1186/s12967-023-04281-6 (2023).
50. de Azevedo, R. A. *et al.* MIF inhibition as a strategy for overcoming resistance to immune checkpoint blockade therapy in melanoma. *OncoImmunology* **9**, 1846915, doi:10.1080/2162402X.2020.1846915 (2020).
51. Iovanna, J. L. & Closa, D. Factors released by the tumor far microenvironment are decisive for pancreatic adenocarcinoma development and progression. *Oncoimmunology* **6**, e1358840, doi:10.1080/2162402x.2017.1358840 (2017).
52. Stamatopoulos, A. *et al.* Mesenchymal stromal cells for bone sarcoma treatment: Roadmap to clinical practice. *Journal of Bone Oncology* **16**, 100231,

doi:https://doi.org/10.1016/j.jbo.2019.100231 (2019).

53. Tang, R. *et al.* Bystander Expression of Atypical Chemokine Receptor 2 Protects T Cells from Chemoattraction towards Cancer-Associated Fibroblasts. *Eur J Immunol* **55**, e202451215, doi:10.1002/eji.202451215 (2025).
54. Wajant, H. & Siegmund, D. TNFR1 and TNFR2 in the Control of the Life and Death Balance of Macrophages. *Frontiers in Cell and Developmental Biology* **Volume 7 - 2019**, doi:10.3389/fcell.2019.00091 (2019).
55. Siegmund, D., Ehrenschwender, M. & Wajant, H. TNFR2 unlocks a RIPK1 kinase activity-dependent mode of proinflammatory TNFR1 signaling. *Cell Death & Disease* **9**, 921, doi:10.1038/s41419-018-0973-3 (2018).
56. Castro, B. A. *et al.* Macrophage migration inhibitory factor downregulation: a novel mechanism of resistance to anti-angiogenic therapy. *Oncogene* **36**, 3749-3759, doi:10.1038/onc.2017.1 (2017).
57. Ghoochani, A. *et al.* MIF-CD74 signaling impedes microglial M1 polarization and facilitates brain tumorigenesis. *Oncogene* **35**, 6246-6261, doi:10.1038/onc.2016.160 (2016).
58. Yaddanapudi, K. *et al.* MIF is necessary for late-stage melanoma patient MDSC immune suppression and differentiation. *The Journal of Immunology* **196**, 74.76-74.76, doi:10.4049/jimmunol.196.Supp.74.6 (2016).
59. Zeiner, P. S. *et al.* Distribution and prognostic impact of microglia/macrophage subpopulations in gliomas. *Brain Pathol* **29**, 513-529, doi:10.1111/bpa.12690 (2019).
60. Liu, Z., Wang, X., Wang, Y. & Zhang, G. Integration analysis of single-cell transcriptome reveals SPP1+ and TFF3+ macrophage subsets contributing to the brain metastasis from lung cancer. *Translational Cancer Research* **14**, 5680-5693 (2025).
61. Liu, M. *et al.* The enhanced cancer nanovaccine by bidirectionally blocking CXCL12/CXCR4 axis to inhibit the recurrence and metastasis of triple-negative breast cancer. *Mol Cancer* **24**, 290, doi:10.1186/s12943-025-02496-3 (2025).
62. Wang, Y., Zhao, Y., Zhou, C. & Wang, Y. Targeting FAP/CAFs to rewire immune-excluded and resistant tumor niches. *Frontiers in Pharmacology* **Volume 17 - 2026**, doi:10.3389/fphar.2026.1812674 (2026).

Figures

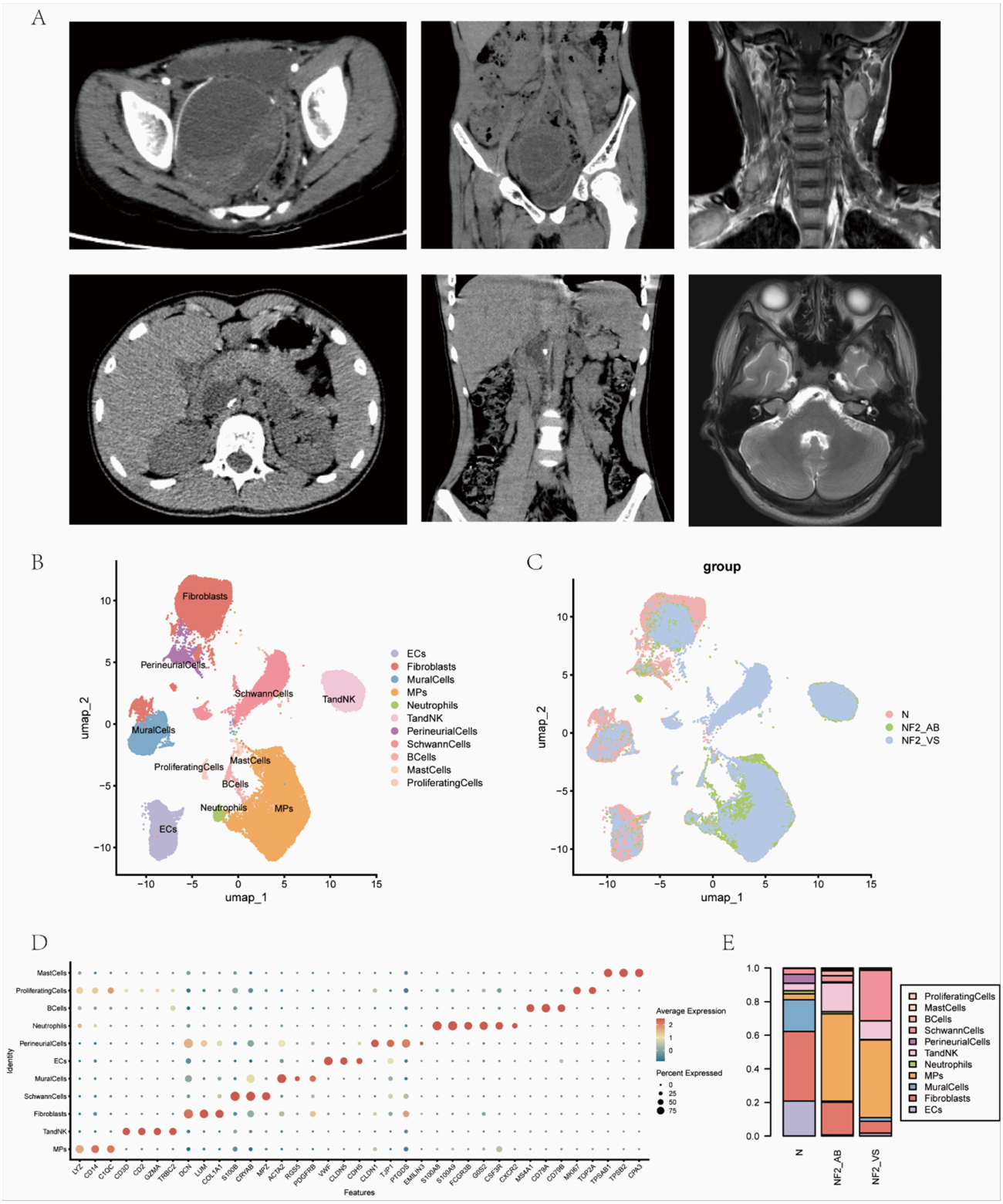


Figure 1

Clinical imaging and single-cell atlas of NF2-associated abdominopelvic schwannomas. (A) Representative CT and MRI images showing abdominopelvic masses and vestibular-nerve lesions in the two patients. (B) UMAP of 61,480 cells colored by major cell class. (C) UMAP colored by normal nerve (N), NF2-associated abdominopelvic tumor (NF2_AB), or NF2-associated vestibular schwannoma

(NF2_VS). (D) Dot plot of canonical markers for the major cell classes. (E) Descriptive cellular composition of the three groups.

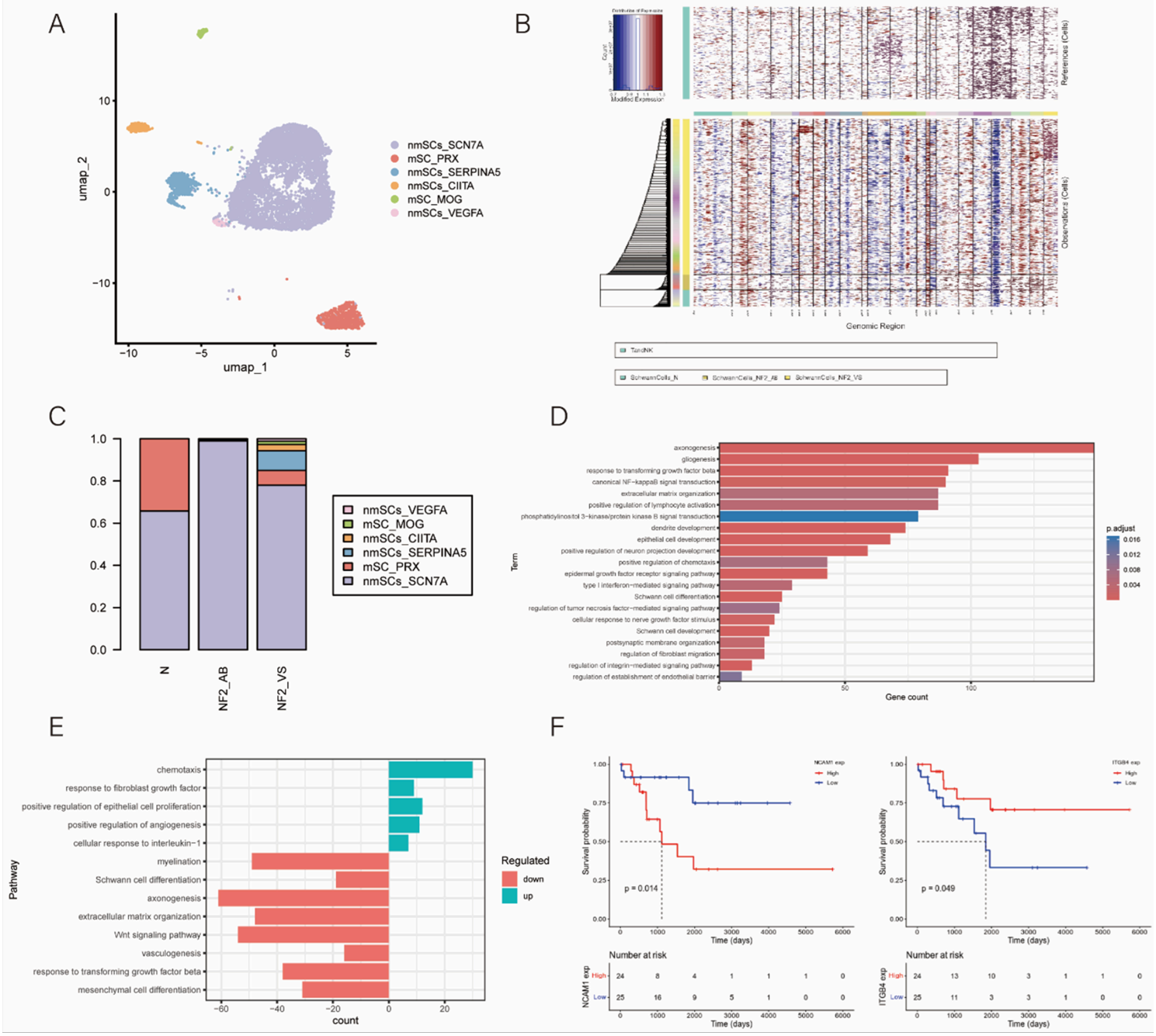


Figure 2

Transcriptional features of tumor-associated Schwann cells across anatomical sites. (A) UMAP of six Schwann-cell populations. (B) inferCNV heatmap using T/NK cells as the reference. (C) Descriptive distribution of Schwann-cell populations across groups. (D) GO enrichment of differentially expressed genes in the nmSC_SCN7A population. (E) Bidirectional enrichment comparison between NF2_AB and NF2_VS; positive values indicate relative enrichment in NF2_AB and negative values indicate relative enrichment in NF2_VS. (F) Exploratory Kaplan-Meier analyses of *NCAM1* and *ITGB4*expression and overall survival in an external cohort.

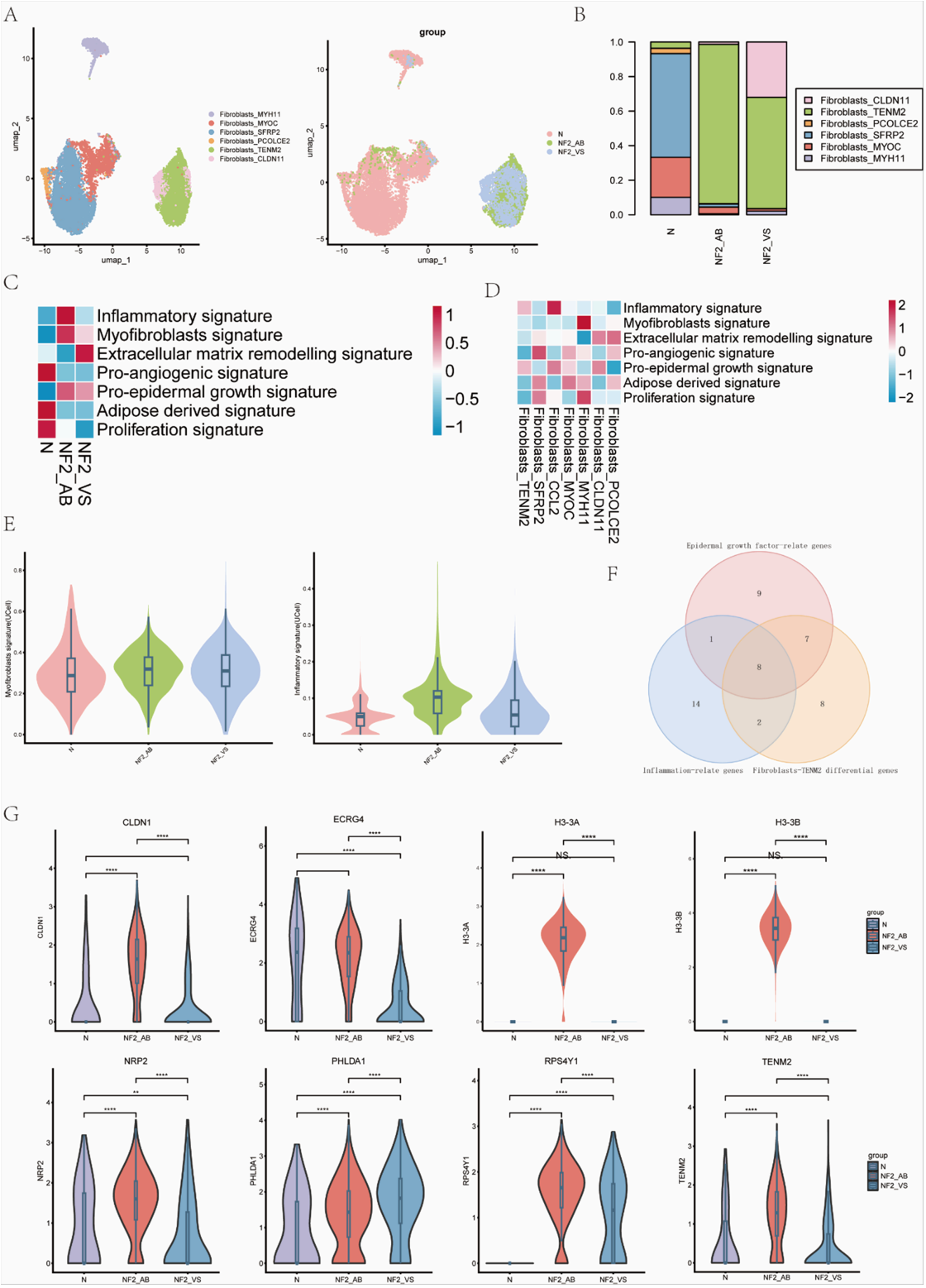


Figure 3

Enrichment and characterization of TENM2-positive fibroblasts in abdominopelvic tumors. (A) UMAPs of fibroblast populations and sample sources. (B) Descriptive distribution of fibroblast populations across groups. (C) Heatmap of fibroblast functional scores across groups. (D) Heatmap of functional scores across fibroblast populations. (E) Myofibroblast-like and inflammatory scores across groups. (F) Intersection of epidermal-growth-related genes, inflammation-related genes, and genes differentially

expressed in TENM2-positive fibroblasts. (G) Expression distributions of eight candidate genes across groups.

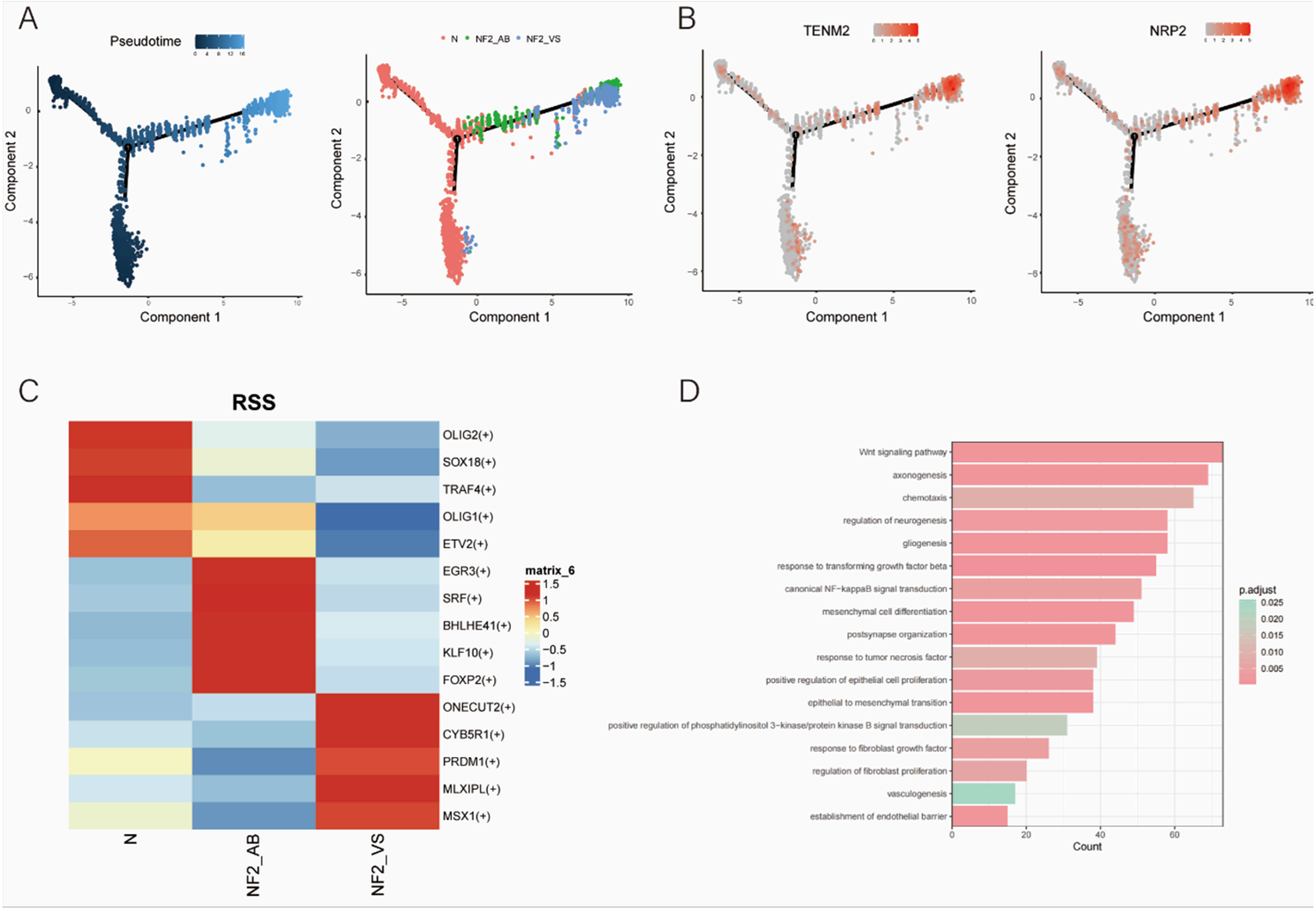


Figure 4

Fibroblast-state trajectory, tissue expression of inflammatory markers, and transcriptional regulatory programs.(A) Fibroblast pseudotime trajectory and group distribution. (B) Expression of *TENM2*and *NRP2* along the trajectory. (C) Regulon Specificity Score heatmap of group-associated regulons. (D) GO enrichment of predicted targets of candidate regulons in abdominopelvic fibroblasts.

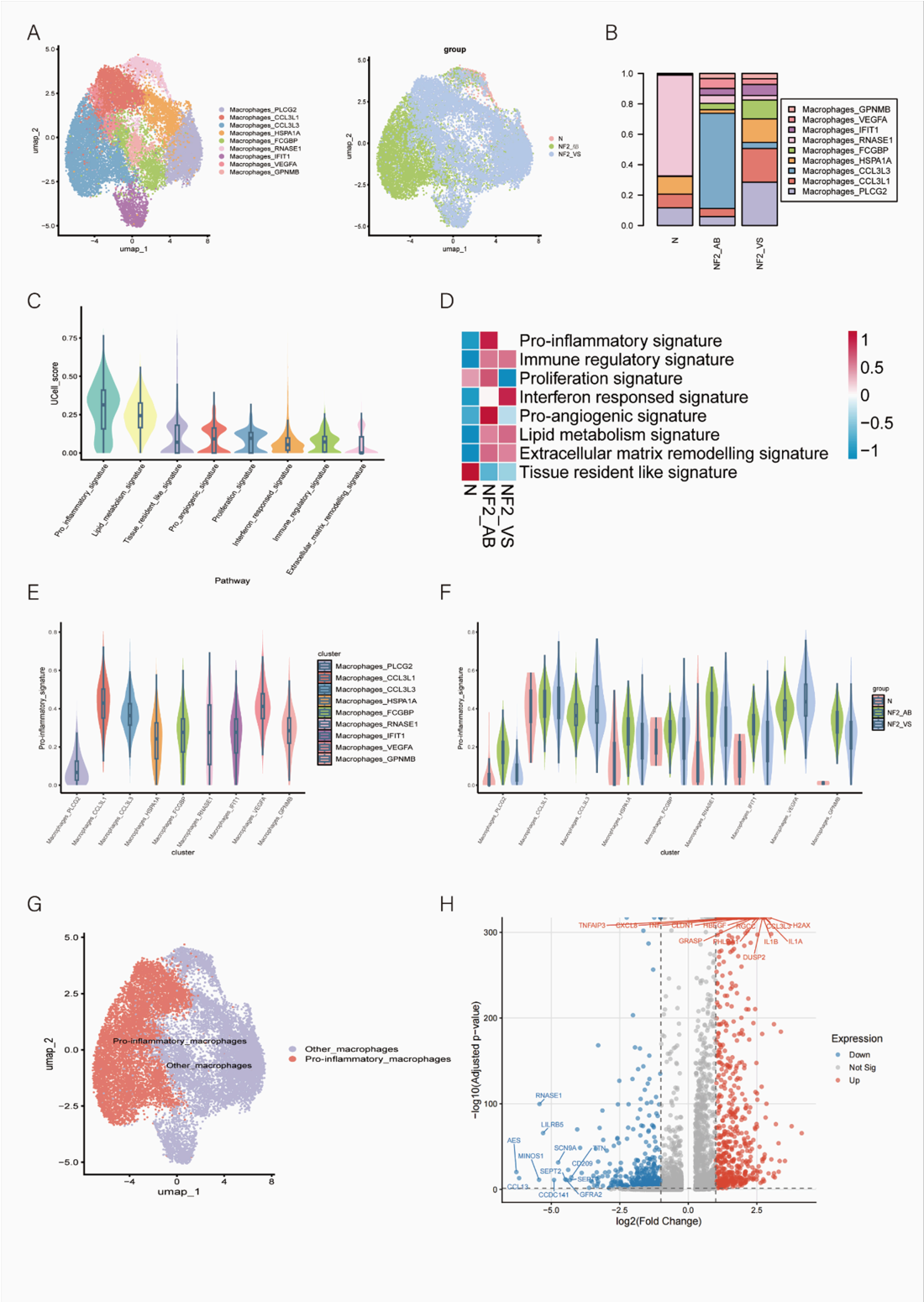


Figure 5

Macrophage heterogeneity and operational definition of inflammation-associated macrophages. (A) UMAPs of nine macrophage populations and their sample sources. (B) Descriptive distribution of macrophage populations across groups. (C) Distribution of macrophage functional scores. (D) Heatmap of macrophage functional scores across groups. (E) Proinflammatory scores across macrophage populations. (F) Population-level proinflammatory scores stratified by group. (G) UMAP of inflammation-

associated and other macrophages. (H) Volcano plot of differential expression between the two macrophage categories.

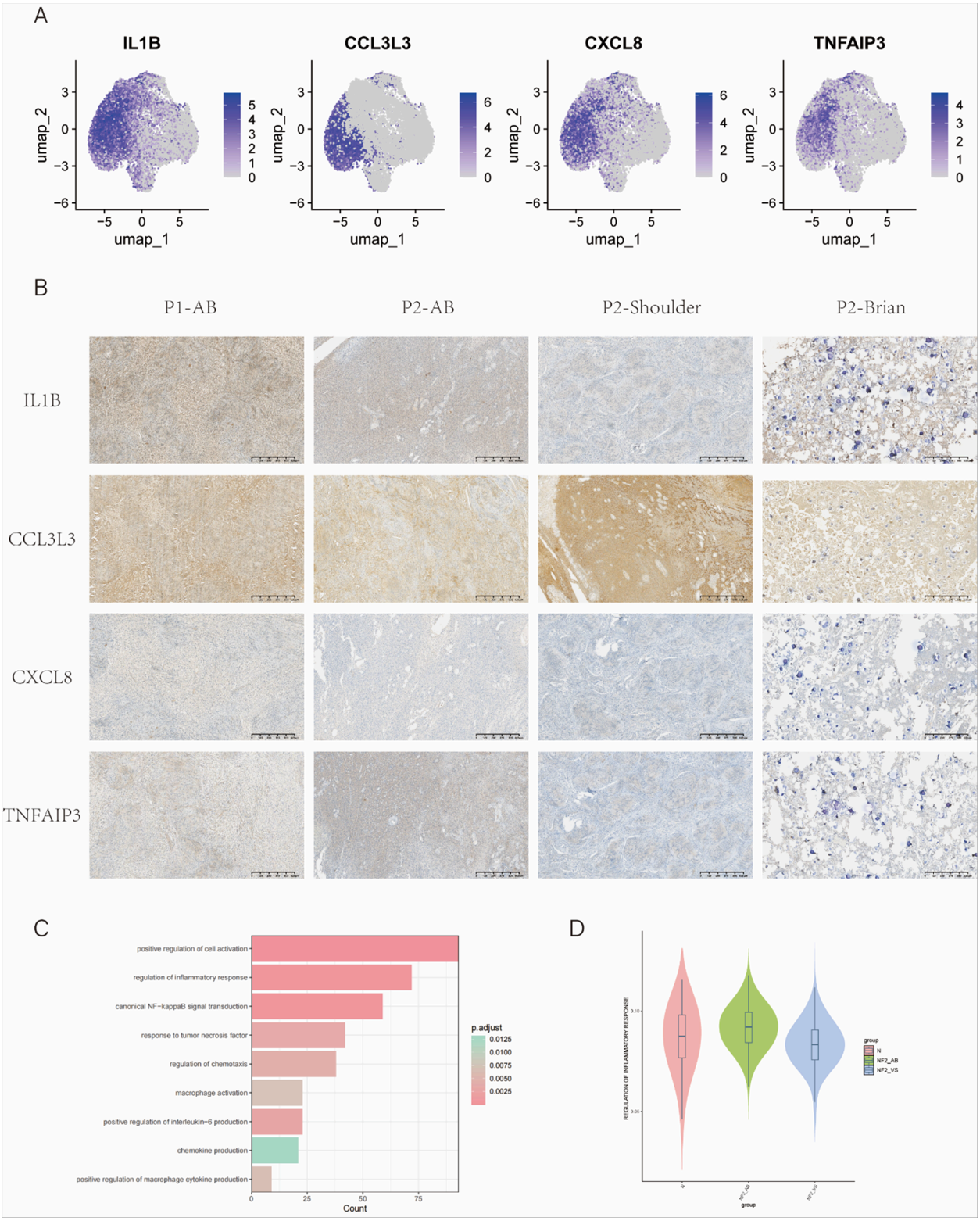


Figure 6

Expression and tissue validation of inflammation-associated myeloid programs. (A) UMAP expression of *IL1B*, *CCL3L3*, *CXCL8*, and *TNFAIP3* in macrophages. (B) Representative immunohistochemical images

of the corresponding proteins in NF2-associated tumors from different sites. (C) GO enrichment of genes upregulated in NF2_AB-derived macrophages relative to NF2_VS-derived macrophages. (D) NF-kappaB-related inflammatory-response scores in monocytes across groups.

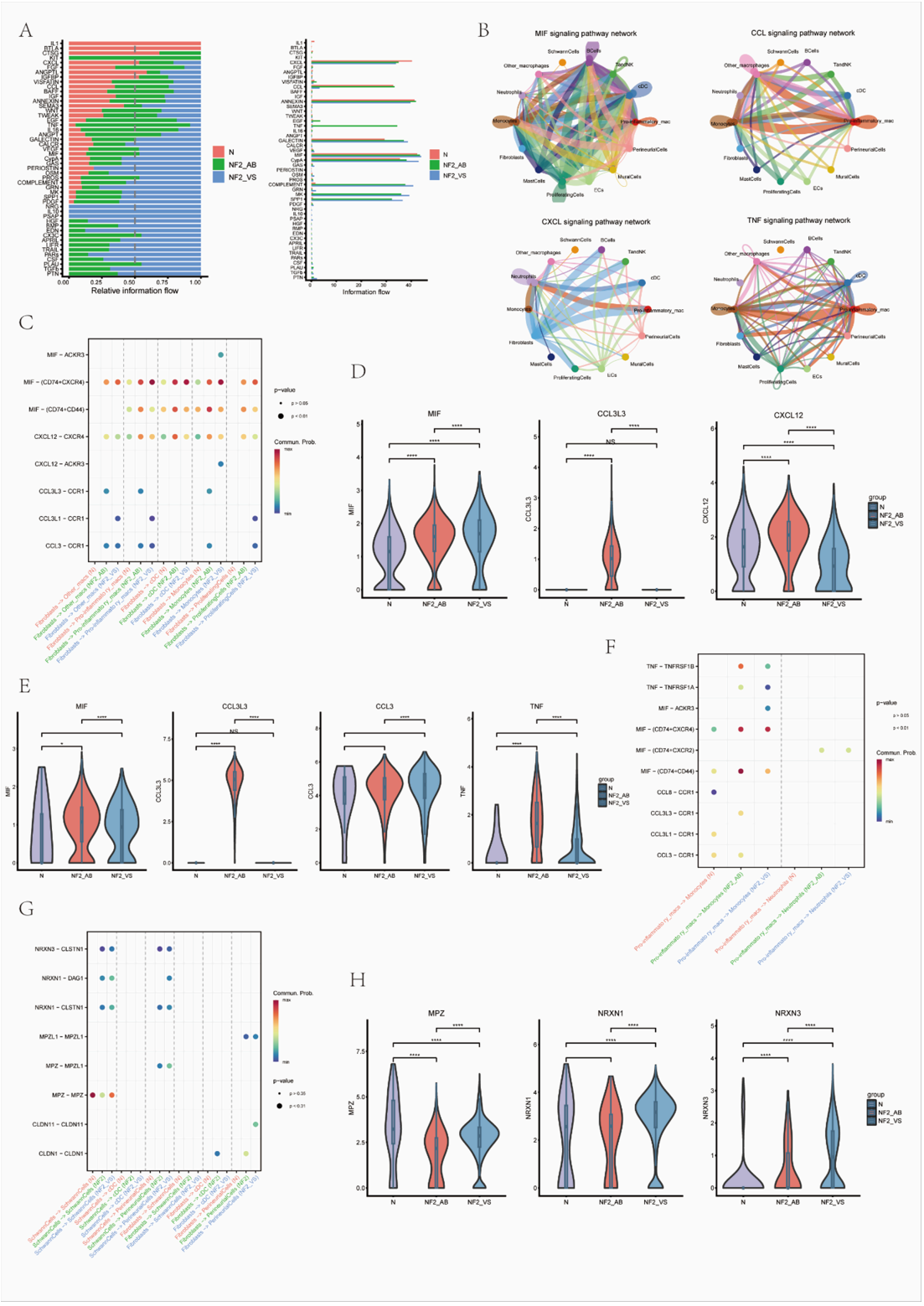


Figure 7

Inferred cell-cell communication networks across anatomical sites. (A) Relative and absolute information flow of secreted signaling pathways. (B) MIF, CCL, CXCL, and TNF signaling networks. (C) Candidate fibroblast-associated ligand-receptor pairs. (D) Group-level expression of *MIF*, *CCL3L3*, and *CXCL12*. (E) Expression of *MIF*, *CCL3L3*, *CCL3*, and *TNF* in inflammation-associated macrophages. (F) Candidate ligand-receptor pairs from inflammation-associated macrophages to myeloid cells. (G) Candidate contact-dependent ligand-receptor pairs involving Schwann cells or fibroblasts. (H) Group-level expression of *MPZ*, *NRXN1*, and *NRXN3*.

Supplementary Files

This is a list of supplementary files associated with this preprint. Click to download.

- image8.png